Biochimica et Biophysica Acta 1798 (2010) 327–337

Contents lists available at ScienceDirect

Biochimica et Biophysica Acta

journal homepage: www.elsevier.com/locate/bbamem

A membranotropic region in the C-terminal domain of Hepatitis C virus protein NS4B Interaction with membranes

Jaime Guillén, Alejandro González-Álvarez, José Villalaín *

Instituto de Biología Molecular y Celular, Universidad Miguel Hernández, E-03202, Elche-Alicante, Spain

ARTICLE INFO

Article history:
Received 5 May 2009
Received in revised form 5 July 2009
Accepted 8 July 2009
Available online 22 July 2009

Keywords:
NS4B
HCV
Lipid–peptide interaction
Membranous web

ABSTRACT

We have identified a membrane-active region in the HCV NS4B protein by studying membrane rupture induced by a NS4B-derived peptide library on model membranes. This segment corresponds to one of two previously predicted amphipathic helix and define it as a new membrane association domain. We report the binding and interaction with model membranes of a peptide patterned after this segment, peptide $NS4B_{H2}$, and show that $NS4B_{H2}$ strongly partitions into phospholipid membranes, interacts with them, and is located in a shallow position in the membrane. Furthermore, changes in the primary sequence cause the disruption of the hydrophobicity along the structure and prevent the resulting peptide from interacting with the membrane. Our results suggest that the region where the $NS4B_{H2}$ is located might have an essential role in the membrane replication and/or assembly of the viral particle through the modulation of the replication complex. Our findings therefore identify an important region in the HCV NS4B protein which might be implicated in the HCV life cycle and possibly in the formation of the membranous web.

1. Introduction

Hepatitis C virus (HCV), an enveloped positive single-stranded RNA virus included in the genus *Hepacivirus*, family *Flaviviridae*, is a major cause of liver disease. With approximately 170 to 200 million people infected worldwide [1,2] and no protective vaccine available at present, this disease has emerged as a serious global health problem since the virus was first identified [3,4]. HCV has a single-stranded genome which encodes a polyprotein of about 3010 amino acids. HCV entry into the host cell is achieved by the fusion of viral and cellular membranes, and the morphogenesis has been suggested to take place in the endoplasmic reticulum [5]. The structural proteins are located in the N-terminal part of the polyprotein and the non-structural proteins (NS) in the latter part [6]. The variability of the HCV proteins gives the virus the ability to escape the host immune surveillance system and notably hampers the development of an efficient vaccine.

Details about HCV replication process remain largely unclear, but it is generally believed that most of the NS proteins are involved. The fact that all NS proteins are localized together with newly synthesized viral RNA on the endoplasmic reticulum (ER) or membranes originating from it [7–9] supports this hypothesis. Most NS proteins also interact with several other NS proteins, and some of them interact with all [10]. The non-structural proteins include two viral proteases, NS2 and NS3, responsible for the maturation of all the NS proteins [11]. The NS4A protein serves as a cofactor for NS3 and is incorporated as an integral component into the enzyme core. NS3 is a multifunctional protein with a RNA helicase/NTPase domain apart from the serine protease domain [12–14]. NS5A is a phosphoprotein of unknown function, but is indispensable for replication and was suggested to be involved in interferon resistance [15–17]. The NS5B RNA-dependent RNA polymerase is the catalytic subunit of the viral replication complex [18–20].

The NS4B protein is a highly hydrophobic poorly characterized protein. Immunofluorescence analyses and subcellular fractionation experiments indicate that NS4B is associated with membranes of the ER or an ER-derived modified compartment [21]. It has recently been shown that NS4B is palmitoylated in the C-terminal region of the protein and its N-terminal cytoplasmic region has potent polymerization activity [22]. NS4B is also engaged in virus assembly and release [23]. Interestingly, the expression of NS4B induces the formation of intracellular membrane changes that are visible by electron microscopy, the so called membranous web [24]. This membranous web has been postulated to be the HCV RNA replication complex. Thus, a function of NS4B might be to induce a specific membrane alteration

Abbreviations: BPI, Bovine brain L-α-phosphadidylinositol; BPS, Bovine brain L-α-phosphatidylserine; CF, 5-Carboxyfluorescein; Chol, Cholesterol; di-8-ANEPPS, 4-(2-(6-(Dioctylamino)-2-naphthalenyl)-(ethenyl)-1-(3-sulfopropyl)-pyridinium inner salt; DMPC, 1,2-Dimyristoyl-*sn*-glycero-phosphatidylcholine; DMPG, 1,2-Dimyristoyl-*sn*-glycero-phosphatidylglycerol; DMPS, 1,2-Dimyristoyl-*sn*-glycero-3-phosphatidylserine; DPH, 1,6-Diphenyl-1,3,5-hexatriene; DSC, Differential Scanning Calorimetry; EPA, Egg L-α-phosphatidic acid; EPC, Egg L-α-phosphatidylcholine; EPG, Egg L-α-phosphatidylglycerol; ER, Endoplasmic reticulum; FD10/20/70, Fluorescein isothiocyanate dextran with an average molecular weight of 10,000/20,000/70,000; HCV, Hepatitis C virus; LUV, Large unilamellar vesicles; MLV, Multilamellar vesicles; NS, Non-structural protein; SC1/2, Scrambled peptide 1/2; SM, Egg sphingomyelin; SUV, Small unilamellar vesicles; TFE, Trifluoroethanol; T_m, Temperature of the gel-to-liquid crystalline phase transition; TM, Transmembrane domain; TMA-DPH, 1-(4-trimethylammoniumphenyl)-6-phenyl-1,3,5-hexatriene; TPE, Egg trans-esterified L-α-phosphatidylethanolamine

* Corresponding author. Tel.: +34 966 658 762; fax: +34 966 658 758.
E-mail address: jvillalain@umh.es (J. Villalaín).

0005-2736/$ – see front matter © 2009 Elsevier B.V. All rights reserved.
doi:10.1016/j.bbamem.2009.07.011

that serves as a scaffold for the formation of the HCV replication complex and therefore has a critical role in the HCV cycle. Due to the high hydrophobic nature of NS4B, a detailed structure determination of this protein using experimental techniques will not be obtained in the near future. Computer analyses and experimental data based on glycosylation mapping predicted four to five transmembrane domains in the NS4B protein with the N terminus in the lumen and the C terminus in the cytoplasm [21,25,26] (see Fig. 1A). The model proposes two conformational states of the N-terminal tail of NS4B, an orientation towards the cytoplasm and a translocation of the NS4B N terminus across the ER membrane with the formation of a fifth transmembrane domain with the N terminus probably located around amino acid 60 [27]. This translocation occurs in all genotypes and can be associated with the membrane-changing capacity of NS4B [27]. Therefore NS4B is likely to be anchored to the membrane and be an integral membrane protein [21]. The C-terminal part of NS4B reveals significant similarities throughout all investigated viruses of the *Flaviviridae* family. Two α-helical elements have been predicted, the first α-helix (H1) being 13 residues in length (approximately from amino acid 1912 to 1924) and the second α-helix (H2) comprising 23 residues (approximately from amino acid 1940 to 1963) pointing out to a yet unknown common function of the C-terminal globular part in *Flaviviridae* [28]. Interestingly, mutations in H2 abolish replication [23,29].

We have recently identified the membrane-active regions of a number of viral proteins by observing the effect of glycoprotein-derived peptide libraries on model membrane integrity [30–34]. These results allowed us to propose the location of different segments in these proteins that are implicated in protein–lipid and protein–protein interactions. These studies have helped us to understand the mechanisms underlying the interaction between viral proteins and membranes. In the present study, we report the binding and interaction of a peptide corresponding to the second of the two predicted amphipathic helices (peptide $NS4B_{H2}$) and define it as a new membrane association domain. We show that $NS4B_{H2}$ strongly partitions into phospholipid membranes, interacts with them, and is located in a shallow position in the membrane. These results would suggest that this NS4B element is an essential constituent of the interaction between the protein and the membrane and might shed light into the specific function of the NS4B protein in the viral cycle.

2. Materials and methods

2.1. Materials and reagents

Three sets of 37 peptides derived from HCV_1aH77 protein NS4B (strictly speaking, NS4B spans from residue 1712 to residue 1972 of the HCV polyprotein precursor) were obtained through the NIH AIDS

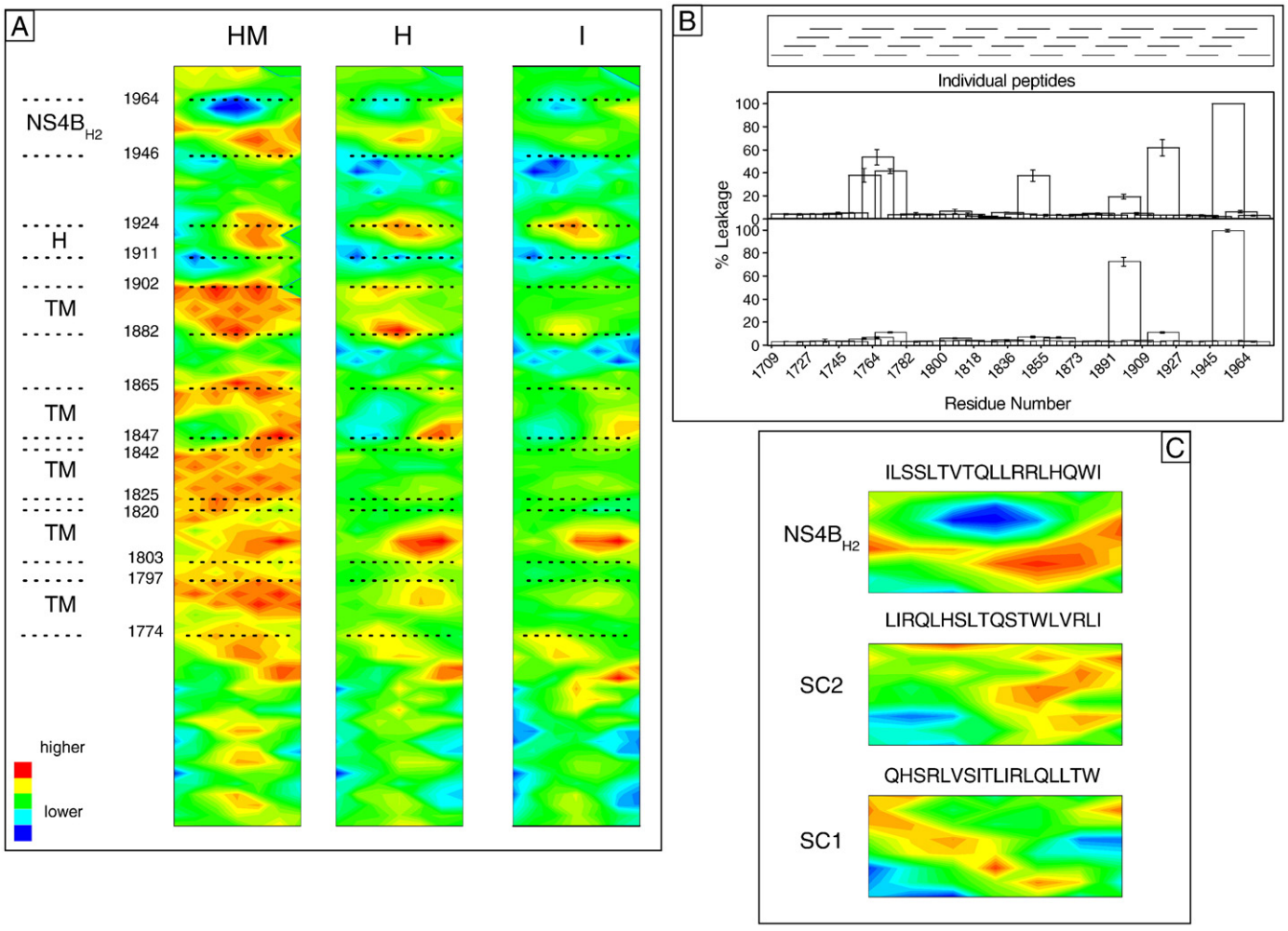

Fig. 1. (A) Hydrophobic moment, hydrophobicity and interfacial hydrophobicity distribution of HCV protein NS4B, assuming it forms an α-helical wheel [31]. The approximate functional regions, according to literature consensus [23,25,28] are also shown: five proposed transmembrane regions (TM) and two putative α-helices, H1 and $NS4B_{H2}$. (B) Correlation of the HCV NS4B derived peptide library with sequence and membrane leakage elicited by the peptide library on model membranes composed of EPC/SM/Chol at a phospholipid molar ratio of 5:1:1, and a complex lipid composition resembling the ER membrane (upper and lower histograms, respectively). Vertical bars indicate standard deviations of the mean of triplicate samples. (C) Sequences and hydrophobic moments of the peptides $NS4B_{H2}$, SC1 and SC2, used in this study, assuming they form an α-helix.

Research and Reference Reagent Program (Division of AIDS, NIAID, NIH, Bethesda, MD). The synthetic peptide encompassing residues 1946–1964 of HCV_1aH77 strain NS4B (^{1946}ILSSLTVTQLLRRLHQWI^{1964}) ($NS4B_{H2}$) and two scrambled versions QHSRLVSITLIRLQLLTW (SC1) and LIRQLHSLTQSTWLVRLI (SC2) were synthesized with N-terminal acetylation and C-terminal amidation on an automatic multiple synthesizer (Genemed Synthesis, San Antonio, TX, USA). The peptides were purified by reverse-phase high-performance liquid chromatography (Vydac C-8 column, 250×4.6 mm, flow rate 1 ml/min, solvent A, 0.1% trifluoroacetic acid, solvent B, 99.9 acetonitrile and 0.1% trifluoroacetic acid) to >95% purity, and its composition and molecular mass were confirmed by amino acid analysis and mass spectroscopy. Since trifluoroacetate has a strong infrared absorbance at approximately 1673 cm^{-1}, which interferes with the characterization of the peptide Amide I band [35], residual trifluoroacetic acid, used both in peptide synthesis and in the high-performance liquid chromatography mobile phase, was removed by several lyophilization/solubilization cycles in 10 mM HCl [36]. Peptide $NS4B_{H2}$ was solubilized in water whereas peptides SC1 and SC2 were solubilized in water/DMSO at 50% (v/v). Bovine brain phosphatidylserine (BPS), bovine liver L-α-phosphatidylinositol (BPI), cholesterol (Chol), egg phosphatidic acid (EPA), egg L-α-phosphatidylcholine (EPC), egg sphingomyelin (SM), egg transesterified L-α-phosphatidylethanolamine (TPE), liver lipid extract, tetramyristoyl cardiolipin (CL), 1,2-dimyristoylphosphatidylserine (DMPS), 1,2-dimyristoylphosphatidylcholine (DMPC) and 1,2-dimyristoylphosphatidylglycerol (DMPG) were obtained from Avanti Polar Lipids (Alabaster, AL, USA). The lipid composition of the synthetic endoplasmic reticulum was EPC/CL/BPI/TPE/BPS/EPA/SM/Chol at a molar ratio of 59:0.37:7.7:18:3.1:1.2:3.4:7.8 [37, 38]. 5-Carboxyfluorescein (CF, >95% by HPLC), 4-(2-(6-(Dioctylamino)-2-naphthalenyl) ethenyl)-1-(3-sulfopropyl)-pyridinium inner salt (di-8-ANEPPS), fluorescein isothiocyanate labeled dextrans (FD-10, FD-20 and FD-70, deuterium oxide (99.9%), Triton X-100, EDTA and HEPES were purchased from Sigma-Aldrich (Madrid, ES). 1,6-Diphenyl-1,3,5-hexatriene (DPH), and 1-(4-trimethylammoniumphenyl)-6-phenyl-1,3,5-hexatriene (TMA-DPH) were obtained from Molecular Probes (Eugene, OR). All other chemicals were commercial samples of the highest purity available (Sigma-Aldrich, Madrid, ES). Water was deionized, twice-distilled and passed through Milli-Q equipment (Millipore Ibérica, Madrid, ES) to a resistivity higher than 18 MΩ cm.

2.2. Vesicle preparation

Aliquots containing the appropriate amount of lipid in chloroform–methanol (2:1 vol/vol) were placed in a test tube, the solvents were removed by evaporation under a stream of O_2-free nitrogen, and finally, traces of solvents were eliminated under vacuum in the dark for >3 h. The lipid films were resuspended in an appropriate buffer and incubated either at 25 °C or 10 °C above the phase transition temperature (T_m) with intermittent vortexing for 30 min to hydrate the samples and obtain multilamellar vesicles (MLV). The samples were frozen and thawed five times to ensure complete homogenization and maximization of peptide/lipid contacts with occasional vortexing. Large unilamellar vesicles (LUV) with a mean diameter of 0.1 μm (leakage measurements) and 0.2 μm (dextran release assays) were prepared from MLV by the extrusion method [39] using polycarbonate filters with a pore size of 0.1 and 0.2 μm (Nuclepore Corp., Cambridge, CA, USA). Small unilamellar vesicles were prepared from MLV using a Branson 250 sonifier (40 W) equipped with a microtip until the suspension became completely transparent. Every 30 s, the samples were cooled for 90 s in ice to prevent overheating of the solution. The titanium particles released from the tip were removed by centrifugation at 15,000 rpm at room temperature for 15 min. For FTIR spectroscopy, aliquots containing the appropriate amount of lipid in chloroform/methanol (2:1, v/v) was placed in a test tube containing 200 μg of dried lyophilized peptide. After vortexing, the solvents were removed by evaporation under a stream of O_2-free nitrogen, and finally, traces of solvents were eliminated under vacuum in the dark for more than 3 h. The samples were hydrated in 100 μl of D_2O buffer containing 20 mM HEPES, 100 mM NaCl, 0.1 mM EDTA, pH 7.4 and incubated at 10 °C above the phase transition temperature (T_m) of the phospholipid mixture with intermittent vortexing for 45 min to hydrate the samples and obtain multilamellar vesicles (MLV). The samples were frozen and thawed as above. Finally the suspensions were centrifuged at 15,000 rpm at 25 °C for 15 min to remove the possible peptide unbound to the membranes. The pellet was resuspended in 25 μl of D_2O buffer and incubated for 45 min at 10 °C above the T_m of the lipid mixture, unless stated otherwise. The phospholipid and peptide concentration were measured by methods described previously [40, 41].

2.3. Membrane leakage and peptide binding to vesicles

LUVs with a mean diameter of 0.1 μm were prepared as indicated above in a buffer containing 10 mM Tris, 20 mM NaCl, pH 7.4, and CF at a concentration of 40 mM. Non-encapsulated CF was separated from the vesicle suspension through a Sephadex G-75 filtration column (Pharmacia, Uppsala, SW, EU) eluted with buffer containing 10 mM Tris, 100 mM NaCl, 1 mM EDTA, pH 7.4. Membrane rupture (leakage) of intraliposomal CF was assayed by treating the probe-loaded liposomes (final lipid concentration, 0.125 mM) with the appropriate amounts of peptide on microtiter plates using a microplate reader (FLUOstar; BMG Labtech, Offenburg, Germany), stabilized at 25 °C with the appropriate amounts of peptide, each well containing a final volume of 170 μl. The medium in the microtiter plates was continuously stirred to allow the rapid mixing of peptide and vesicles. In the case of LUVs (0.2 μm) encapsulated with fluorescent dextrans (FD10, FD20 or FD70) the lipid was resuspended to a concentration of 100 mg/ml solution of dextrans in a buffer containing 10 mM Tris, 100 mM NaCl, pH 7.4. Non-encapsulated dextrans were removed by gel-filtration chromatography using a pump P-50 (Amershan Pharmacia Biotech AB, Uppsala, Sweden) with a Sephacryl® 500-HR column eluted with the same buffer as described above, at a flow rate of 3 ml/min. The final lipid concentration was 0.075 mM in a 5 mm×5 mm fluorescence cuvette (final volume of 400 μl), stabilized at 25 °C and under constant stirring. The fluorescence was measured using a Varian Cary Eclipse spectrofluorimeter. Changes in fluorescence intensity were recorded with excitation and emission wavelengths set at 492 and 517 nm, respectively. Excitation and emission slits were set at 5 nm. Leakage was quantified on a percentage basis as previously described [42,43]. Peptide partitioning into membranes was evaluated by the enhancement of the tryptophan fluorescence by successive additions of small volumes of LUV to a peptide sample (3.4×10^{-5} M). Fluorescence spectra were recorded in a SLM Aminco 8000C spectrofluorometer with excitation and emission wavelengths of 290 and 348 nm, respectively, and 4 nm spectral bandwidths. Measurements were carried out in 10 mM Tris, 100 mM NaCl, EDTA 0.1 mM, pH 7.4. Intensity values were corrected for dilution, and the scatter contribution was derived from lipid titration of a vesicle blank. The peptide concentration in the assays was 30 μm. The data were analyzed as previously described [43].

2.4. Acrylamide quenching of Trp emission and steady-state fluorescence anisotropy

Aliquots from a 4 M solution of the water-soluble quencher were added to the solution-containing peptide in the presence and absence of liposomes at a peptide/lipid molar ratio of 1:70. The results obtained were corrected for dilution and the scatter contribution was derived from acrylamide titration of a vesicle blank. The data were analyzed according to the Stern–Volmer equation [44]. Aliquots of TMA-DPH or DPH in N,N′-dimethylformamide were directly added

into MLVs formed in 10 mM Tris, 100 mM NaCl, EDTA 0.1 mM, pH 7.4 to obtain a probe/lipid molar ratio of 1/500. Samples were incubated for 15 or 60 min when TMA-DPH or DPH were used, respectively, 10 °C above the gel-to-liquid crystalline phase transition temperature T_m of the phospholipid mixture. Afterwards, the peptides were added to obtain a peptide/lipid molar ratio of 1:15 and incubated 10 °C above the T_m of each lipid for 1 h, with occasional vortexing. All fluorescence studies were carried using 5 mm×5 mm quartz cuvettes in a final volume of 400 μl (315 μM lipid concentration). The steady-state fluorescence anisotropy was measured with an automated polarization accessory using a Varian Cary Eclipse fluorescence spectrometer, coupled to a Peltier for automatic temperature change. Samples were excited at 360 nm (slit width, 5 nm) and fluorescence emission was recorded at 430 nm (slit width, 5 nm).

2.5. Differential scanning calorimetry

MLVs were formed as stated above in 20 mM HEPES, 100 mM NaCl, 0.1 mM EDTA, pH 7.4. The peptide was added to obtain a peptide/lipid molar ratio of 1:15. The final volume was 1.2 ml (0.5 mM lipid concentration), and incubated 10 °C above the T_m of each phospholipids for 1 h with occasional vortexing. Samples were loaded into the calorimetric cell. DSC experiments were performed in a VP-DSC differential scanning calorimeter (MicroCal LLC, MA) under a constant external pressure of 30 psi in order to avoid bubble formation, and samples were heated at a constant scan rate of 60 °C/h. Experimental data were corrected from small mismatches between the two cells by subtracting a buffer baseline prior to data analysis. The excess heat capacity functions were analyzed by using Origin 7.0 (Microcal Software). The thermograms were defined by the onset and completion temperatures of the transition peaks obtained from heating scans. In order to avoid artifacts due to the thermal history of the sample, the first scan was never considered; second and further scans were carried out until a reproducible and reversible pattern was obtained.

2.6. Infrared spectroscopy

Infrared spectroscopy measurements were performed and analyzed as described previously [42]. Two-dimensional correlation analysis was carried out using the 2D-Shige program written by Shigeaki Morita and Yukihiro Ozaki (Kwansei-Gakuin University, Japan; http://sci-tech.ksc.kwansei.ac.jp/~ozaki/e_2D.htm). To obtain the 2D-infrared maps, heating was used as the perturbation to induce time-dependent spectral fluctuations in the infrared spectra of DMPC/NS4B peptide and DMPG/NS4B peptide complexes, so that to induce the phase transition of the phospholipid membranes and observe any modulation of the conformation on the peptide induced by the phase change. Visualization of the 2D-infrared maps was performed using Origin software (Microcal Systems, Boulder, CO). The maximum and minimum intensities for the whole correlation map were found, their values were multiplied by two and a maximum of thirty contour lines were drawn, so that the number of contour lines reflects their intensities in relation to the main peak. Since the synchronous spectrum is always required for the interpretation of intensity and width changes, and our interest aims to find the inter-molecular interactions between NS4B peptide and the phospholipids molecules, we have used throughout this work the synchronous 2D-infrared correlation contour maps to analyze the data as it has been done before [45].

2.7. Circular dichroism measurements

Circular dichroism spectra were recorded at 25 °C using a JASCO-810 spectropolarimeter in a 2 mm path-length quartz cell. An external bath circulator Neslab RTE-111, connected to the spectropolarimeter, controlled the sample temperature. Wavelength spectra were acquired every 0.2 nm at a scan speed of 50 nm min^{-1} with a response time of 2 s and averaged over five scans from 250 to 190 nm, with a band width of 2 nm. Spectra were corrected for the blank. Samples contained 6×10^{-5} M of peptide in 10 mM phosphate buffer at pH 7.4. Different concentrations of TFE, DMPC and DMPG were added to the corresponding peptide samples.

3. Results

The analysis of hydrophobicity, hydrophobic moments and interfacial hydrophobicity distribution along the NS4B sequence of HCV_1aH77 strain, assuming an α-helix, is shown in Fig. 1A [31,46,47]. It is possible to observe the highly hydrophobic nature of the protein since 4/5 transmembrane domains, corresponding with the TM proposed domains, are easily apparent [21,25,26]. Furthermore, two zones of highly hydrophobic character, corresponding with the proposed H1 and H2 helices, can be discerned [28] (Fig. 1A). The three dimensional structure of the NS4B protein is not known, but this analysis renders to us the potential surface zones potentially implicated in the modulation of membrane binding. Therefore, these regions could mediate the interaction with similar domains of other HCV NS proteins or with the membrane.

We have studied the effect of a HCV_1aH77 NS4B derived peptide library on membrane rupture by monitoring leakage from two different liposome compositions (Fig. 1B). The peptide library used in this study and their correlation with the HCV NS4B protein sequence is also depicted in Fig. 1B. Two and three consecutive peptides in the library have an overlap of 11 and 4 amino acids, respectively. The lipidic composition of the model membranes was EPC/SM/Chol at a phospholipid molar ratio of 5:1:1, and a complex lipid composition resembling the ER membrane. When the NS4B derived peptide library was assayed on liposomes, some exerted an important leakage effect (Fig. 1B). However, the most remarkable effect was observed for peptide encompassing residues 1946–1964, which produced leakage values of 100%, on the two specific lipid composition tested. Other peptides elicited leakage values between 20 and 70%, but no one was capable of producing 100% leakage values as peptide 1946–1964 did. However, remarkable is the effect of peptide 1891–1909 in ER membranes (peptide 1891–1909 would correspond to a TM proposed domain) and peptide 1913–1929 in the mixture of EPC/SM/Chol (peptide 1913–1929 would correspond to the first putative α-helix). It is interesting to note that peptide corresponding to sequence 1946–1964 of the NS4B protein coincides with the region where the predicted H2 helix resides (see above). As shown in Table 1, this region is significantly conserved among the major genotypes of HCV. The conservation of this pattern across different strains of HCV indicates that this sequence is likely to be an important region in this protein. Taking into account these results, we performed an in-depth study of peptide 1946–1964, i.e., peptide $NS4B_{H2}$, as well as

Table 1
Result of the alignment (ClustalW) of residues 1712–1972 (1aH77 numbering) from reference strains representing the major genotypes of Hepatitis C virus as well as the $NS4B_{H2}$ sequence examined in this work.

Genotype	Virus strain	Sequence
1a	1	ILSSLTVTQLLRRLHQWI
1a	H	ILSSLTVTQLLRRLHQWI
1b	HC-J1	ILSSLTVTQLLRRLHQWL
1b	HC-J4	ILSSLTITQLLKRLHQWI
4a	ED43	ILSSLTVTSLLRRLHKWI
3a	k3a	LLSSLTVTSLLRRLHQWI
3k	JK049	LLSSLTVTQLLRRLHQWI
5a	SA13	LLSSLTVTSLLKRLHTWI
6a	EUHK2	ILTSLTITSLLRRLHQWV
2a	HC-J6	LLGSLTITSLLRRLHNWI
2a	JFH-1	LLGSLTITSLLRRLHNWI
2b	HC-JB	VLSSLTITSLLRRLHAWI
$NS4B_{H2}$		ILSSLTVTQLLRRLHQWI
Consensus		:* ***:*.**:*** *:

The consensus sequence is shown beneath the alignment.

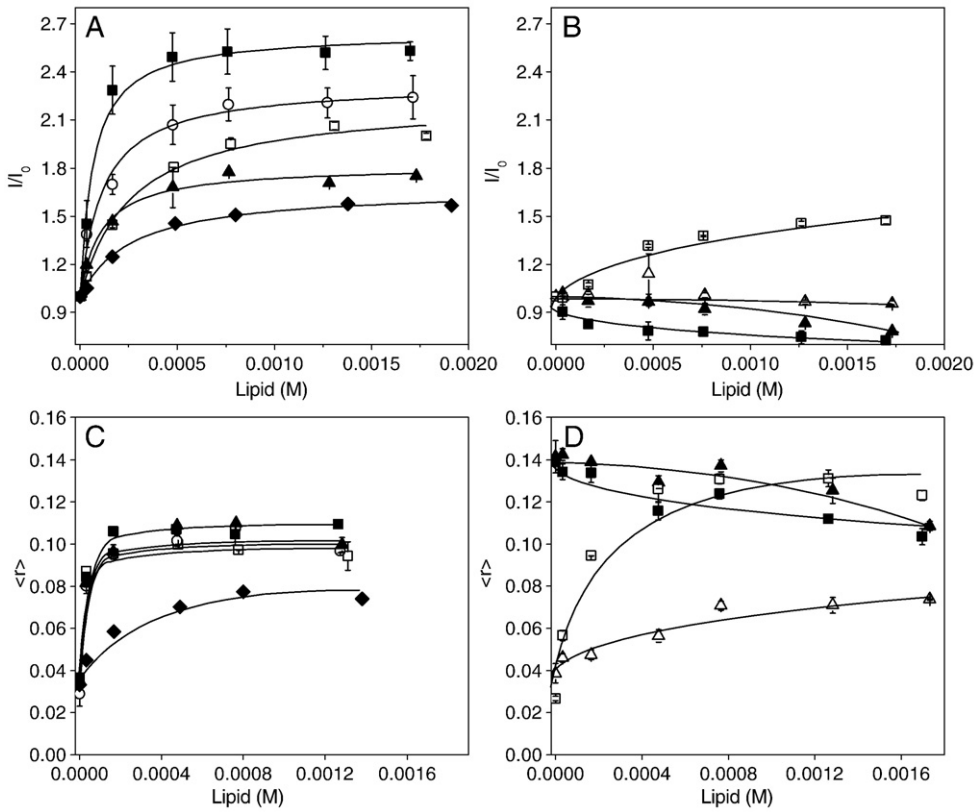

Fig. 2. Change on the fluorescence intensity (A and B) and steady-state anisotropy (C and D) of the Trp residue of the $NS4B_{H2}$ peptide (A and C) and the two scrambled peptides (B and D) in the presence of increasing lipid concentrations. The lipid compositions used were EPC/SM/CHOL at a molar ratio of 5:1:1) (□), EPC/TPE/CHOL at a molar ratio of 5:3:1 (○), synthetic ER membranes (♦) EPC/CHOL at a molar ratio of 5:1, (▲for $NS4B_{H2}$ and SC1 and △ for SC2) and EPC/BPS/CHOL at a molar ratio of 5:3:1 (■ for $NS4B_{H2}$ and SC1 and □ for SC2). To guide the eye empirical lines have been drawn in B, C and D.

two scrambled peptides, SC1 and SC2 (Fig. 1C). We investigated its binding and interaction with different membrane model systems, as well as characterized the structural changes taking place in both the peptide and phospholipid molecules.

The ability of the $NS4B_{H2}$ peptide to interact with membranes was determined from fluorescence studies of the peptide intrinsic Trp in presence of model membranes [48] containing different phospholipid compositions at different lipid/peptide ratios (Fig. 2). The Trp fluorescence intensity of the $NS4B_{H2}$ peptide increased upon increasing the lipid/peptide ratio, indicating a significant change on the environment of the Trp moiety of the peptide (Fig. 2A). However, when the two scrambled peptides SC1 and SC2 were used, also differences were observed since fluorescence intensity increased but slightly in the case of SC2 peptide, and in the presence of the negatively charged phospholipid BPS (Fig. 2B). In the case of the $NS4B_{H2}$ peptide, partition constant (K_p) values in the range 10^5 were obtained for the different phospholipid compositions studied, indicating that the peptide was bound to the membrane surface with high affinity [48–51]. The highest K_p value, i.e., 8.5×10^5, was obtained for the sample containing EPC/BPS/Chol at a molar ratio of 5:3:1 (Fig. 2A). In the presence of membranes,

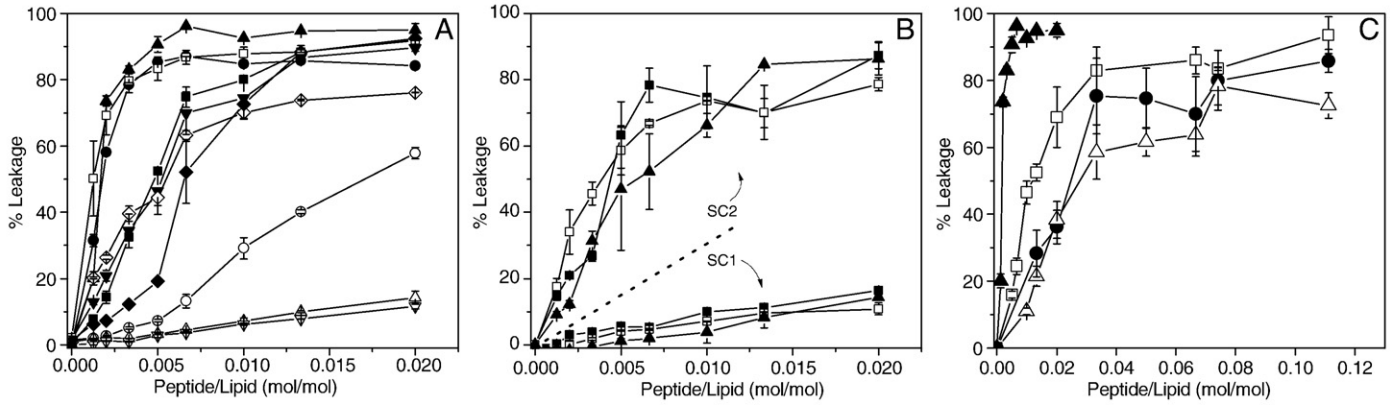

Fig. 3. Effect on the carboxyfluorescein release of LUVs contents for different lipid compositions of the $NS4B_{H2}$ peptide (A) and the SC1 and SC2 peptides (B). The lipid compositions used were EPC (●), EPC/CHOL at a molar ratio of 5:1 (▲), EPC/SM/CHOL at a molar ratio of 2:1:1 (◇), EPC/SM/CHOL at a molar ratio of 5:1:1 (□), EPC/SM/CHOL at a molar ratio of 1:1:1 (▼), EPC/BPS/CHOL at a molar ratio of 5:3:1 (■), EPC/TPE/CHOL at a molar ratio of 5:3:1 (○), EPA/CHOL at a molar ratio of 5:1 (△), lipidic liver extract (▽),and synthetic ER membranes (♦). (C) Effect of the $NS4B_{H2}$ peptide on the release of fluorescein-labeled dextrans, FD-10 (□), FD-20 (●) and FD-70 (△) from LUVs of EPC/Chol at a molar ratio of 5:1. Release of carboxyfluorescein is showed for comparison (▲).

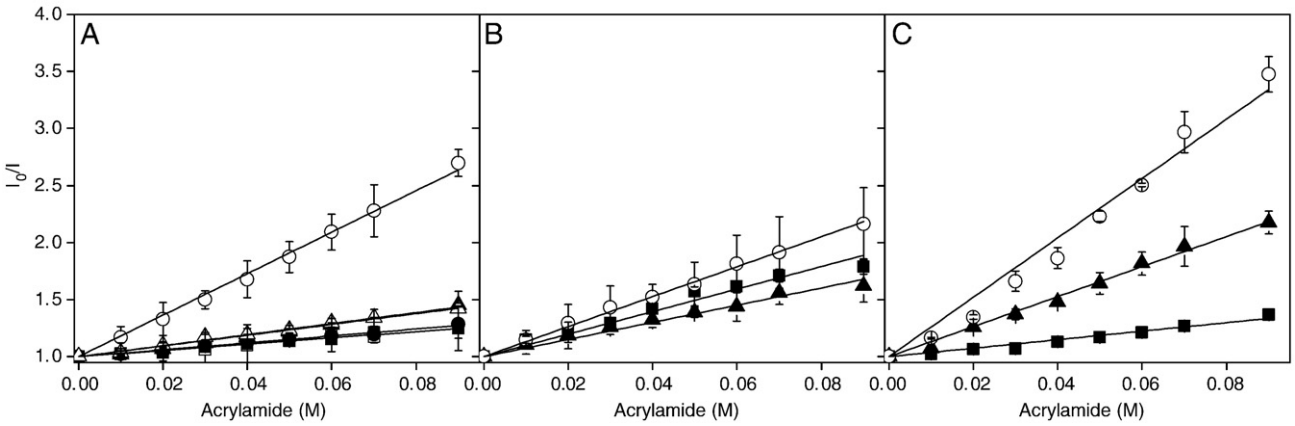

Fig. 4. Stern–Volmer plots for the quenching of the fluorescence of the Trp residue of the (A) $NS4B_{H2}$, (B) SC1 and (C) SC2 peptides by acrylamide. Peptides in buffer (○) and in the presence of LUVs composed of EPC/CHOL at a molar ratio of 5:1 (▲),EPC/BPS/CHOL at a molar ratio of 5:3:1 (■),EPC/TPE/CHOL at a molar ratio of 5:3:1 (○),EPC/SM/CHOL at a molar ratio of 5:1:1 (□) and synthetic ER membranes (♦).

the emission maximum of Trp of the $NS4B_{H2}$ peptide underwent a blue-shift from 350 to 337 nm (not shown). However, the emission maximum of the SC1 peptide remained virtually unaltered at 345 nm and the emission maximum wavelength of the SC2 peptide changed from 350 to 342 in the presence of the zwitterionic lipidic mixture EPC/Chol, and from 350 to 332 in the presence of the negatively charged lipidic mixture EPC/BPS/Chol. Differences in the fluorescence anisotropy values of the peptides were also observed when in the presence of phospholipid model membranes. It was found that addition of liposomes to the $NS4B_{H2}$ and SC2 (Fig. 2D) peptides increased significantly the Trp anisotropy values (Fig. 2C), being greater when negatively charged phospholipids were used in the mixture for SC2 peptide. These results indicate a decrease in the mobility of the Trp residue in these peptides. However, peptide SC1 displayed a high, nearly constant, anisotropy values, indicating, first, a high degree of immobilization (oligomerization/aggregation), even in the absence of membranes, and second, that it was not bound to the membranes (Fig. 2D). Changes on the membrane dipole potential magnitude elicited by $NS4B_{H2}$ was monitored by means of the spectral shift of the fluorescence probe di-8-ANEPPS [52–54]. In the presence of the peptide, the greater decrease in the $R_{450/520}$ value was measured in the presence of negatively charged lipid compositions (not shown for briefness), confirming the presence of a specific interaction of the peptide with vesicles bearing negatively charged phospholipids, demonstrating that the peptide was capable of inserting into the lipid bilayer and modifying the dipole potential.

To explore the effect of the $NS4B_{H2}$ peptide in the destabilization of membrane vesicles, we studied its effect on the release of the encapsulated fluorophores CF, FD10, FD20 and FD70 (Stokes radius around 6 Å, 23 Å, 33 Å and 60 Å, respectively) in model membranes [55,56]. The extent of CF leakage observed at different peptide to lipid molar ratios and the effect on different phospholipid compositions is shown in Fig. 3A where it can be seen that the peptide was able to induce the release of the internal contents of the liposomes in a dose-dependent manner. It is interesting to note that the $NS4B_{H2}$ peptide induced a high percentage of leakage (80–90%), even at lipid/peptide ratios as high as 200:1, for liposomes composed of EPC/Chol at a molar ratio of 5:1, EPC/SM/Chol at a molar ratio of 5:1:1 and EPC (Fig. 3A). Lower, but significant, leakage values were obtained for liposomes composed of EPC/BPS/Chol at a molar ratio of 5:3:1 and EPC/SM/Chol at a molar ratio of 1:1:1 and 2:1:1 (at a lipid/peptide ratio of 200:1 leakage values were about 45–55%). Lower values were obtained for liposomes composed of the synthetic ER membranes, EPC/TPE/Chol at a molar ratio of 5:3:1, EPA/Chol at a molar ratio of 5:1 and a lipidic liver extract. The leakage values observed for the scrambled peptides SC1 and SC2 were much lower as observed in Fig. 2B. For liposomes composed of EPC/BPS/Chol at a molar ratio of 5:3:1, EPC/Chol at a molar ratio of 5:1 and EPC/SM/Chol at a molar ratio of 5:1:1, leakage values at lipid/peptide of 200:1 were about 45–60% for peptide SC2 and about 1–5% for peptide SC1, demonstrating that peptide $NS4B_{H2}$ interacts more significantly with liposomes than the scrambled peptides SC1 and SC2. In order to characterize the pore size of the pores which would be formed by the $NS4B_{H2}$ peptide, we carried out a series of experiments using FITC-dextrans of different sizes entrapped in liposomes composed of EPC/Chol (Fig. 3C). As observed in the figure, $NS4B_{H2}$ was capable of inducing leakage of all fluorophores, albeit at different rates (the smaller the size, the higher the rate of leakage). However, at the highest peptide/lipid ratio used, $NS4B_{H2}$ was capable of releasing a significant percentage of the dextrans (between 70 and 90%) (Fig. 3C). The capacity of the $NS4B_{H2}$ peptide to induce the leakage of the dextrans but at a higher rate for lower size fluorophores and vice versa demonstrates that the $NS4B_{H2}$ peptide is capable of forming pores in the membrane but leading to a complete disruption of the membrane [57,58].

To assess the accessibility of the Trp residue of the $NS4B_{H2}$ peptide to the aqueous environment before and after binding to membranes, acrylamide, an efficient water-soluble neutral quencher probe, was used. Stern–Volmer plots for the quenching of Trp by acrylamide, recorded in the absence and presence of lipid vesicles, are shown in Fig. 4 and the resultant Stern–Volmer constants are presented in Table 2. In aqueous solution the Trp residues were highly exposed to the solvent that led to a more efficient quenching. For the $NS4B_{H2}$ peptide and in the presence of the phospholipid membranes, the extent of quenching was significantly reduced (from a K_{SV} value of 18.19 M^{-1} in buffer to approximately 4.8–2.7 M^{-1} in the presence of membranes). This data would indicate a very poor accessibility of the Trp residues to the aqueous phase, consistent with the incorporation of the peptide into the lipid bilayer. In the case of the scrambled peptides different effects were observed (Fig. 4B and C). The SC1 peptide in solution gave a K_{SV} of 13.15 M^{-1}, suggesting a lesser accessibility of the peptide Trp to the solvent than the $NS4B_{H2}$ peptide

Table 2
Acrylamide Stern–Volmer quenching constants (K_{SV}) obtained from the fluorescence of the Trp residue of the $NS4B_{H2}$, SC1 and SC2 peptides in buffer and in the presence of different model membranes.

LUV compositions	$NS4B_{H2}$	SC1	SC2
EPC/SM/CHOL 5:1:1	2.74	–	–
EPC/TPE/CHOL 5:3:1	3.04	–	–
EPC/BPS/CHOL 5:3:1	2.75	9.86	3.73
EPC/CHOL 5:1	4.71	7.53	13.16
ER	4.83	–	–
Peptide in buffer	18.19	13.15	26.03

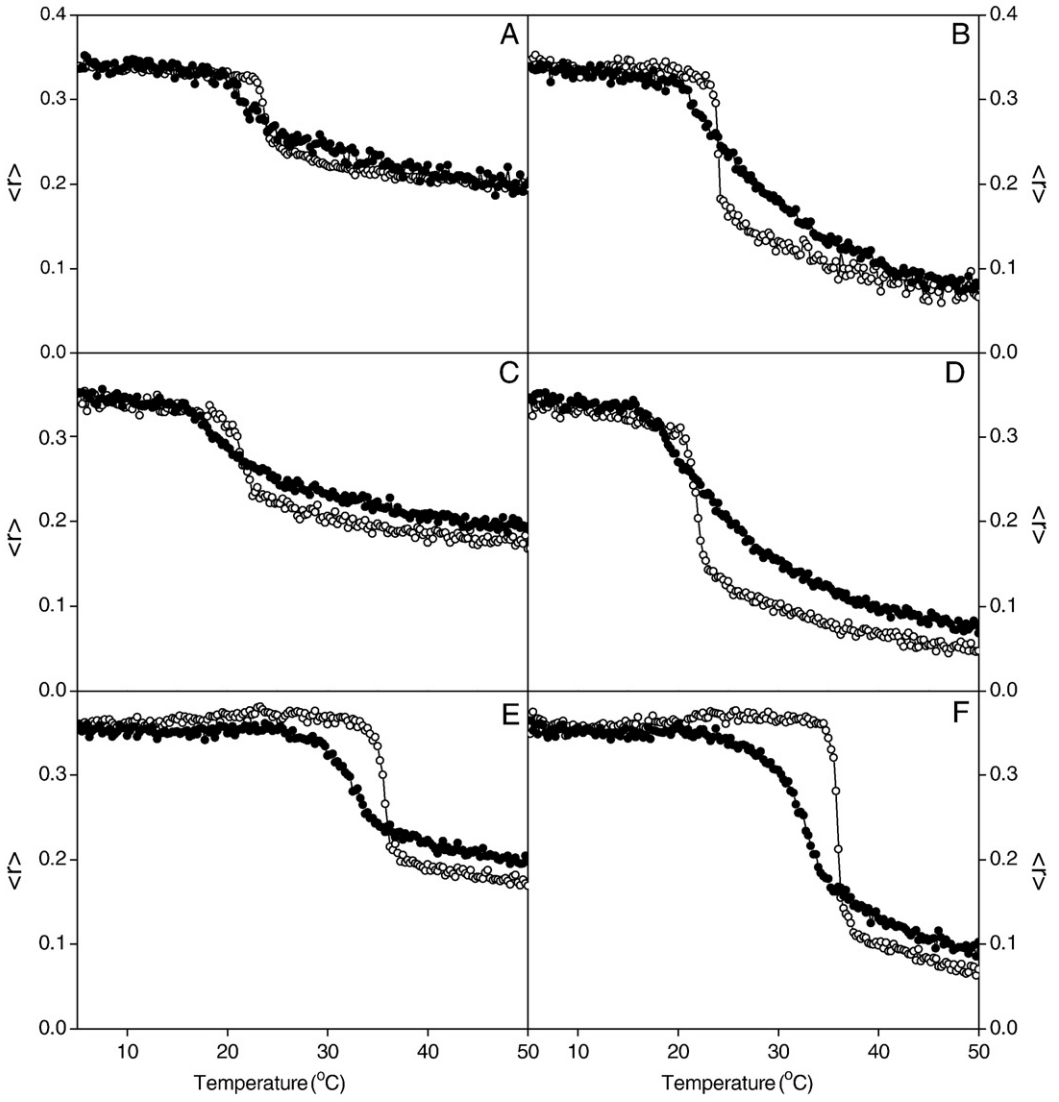

Fig. 5. Steady-state anisotropy, <r>, of DPH (A, C, and E) and TMA-DPH (B, D and F) incorporated into (A and B) DMPC, (C and D) DMPG and (E and F) DMPS model membranes as a function of temperature. Data correspond to vesicles containing pure phospholipid (○) and phospholipid plus $NS4B_{H2}$ peptide at a 15:1 molar ratio (●).

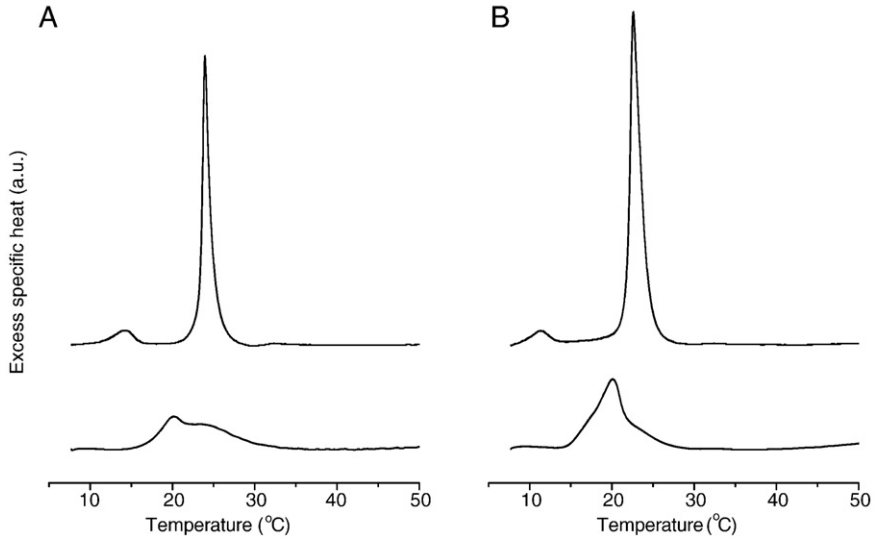

Fig. 6. DSC heating thermograms for liposomes of (A) DMPC and (B) DMPG in the presence (lower curves) and absence (upper curves) of the $NS4B_{H2}$ peptide at a phospholipid/peptide molar ratio of 15:1. All the thermograms are normalized to the same amount of lipid.

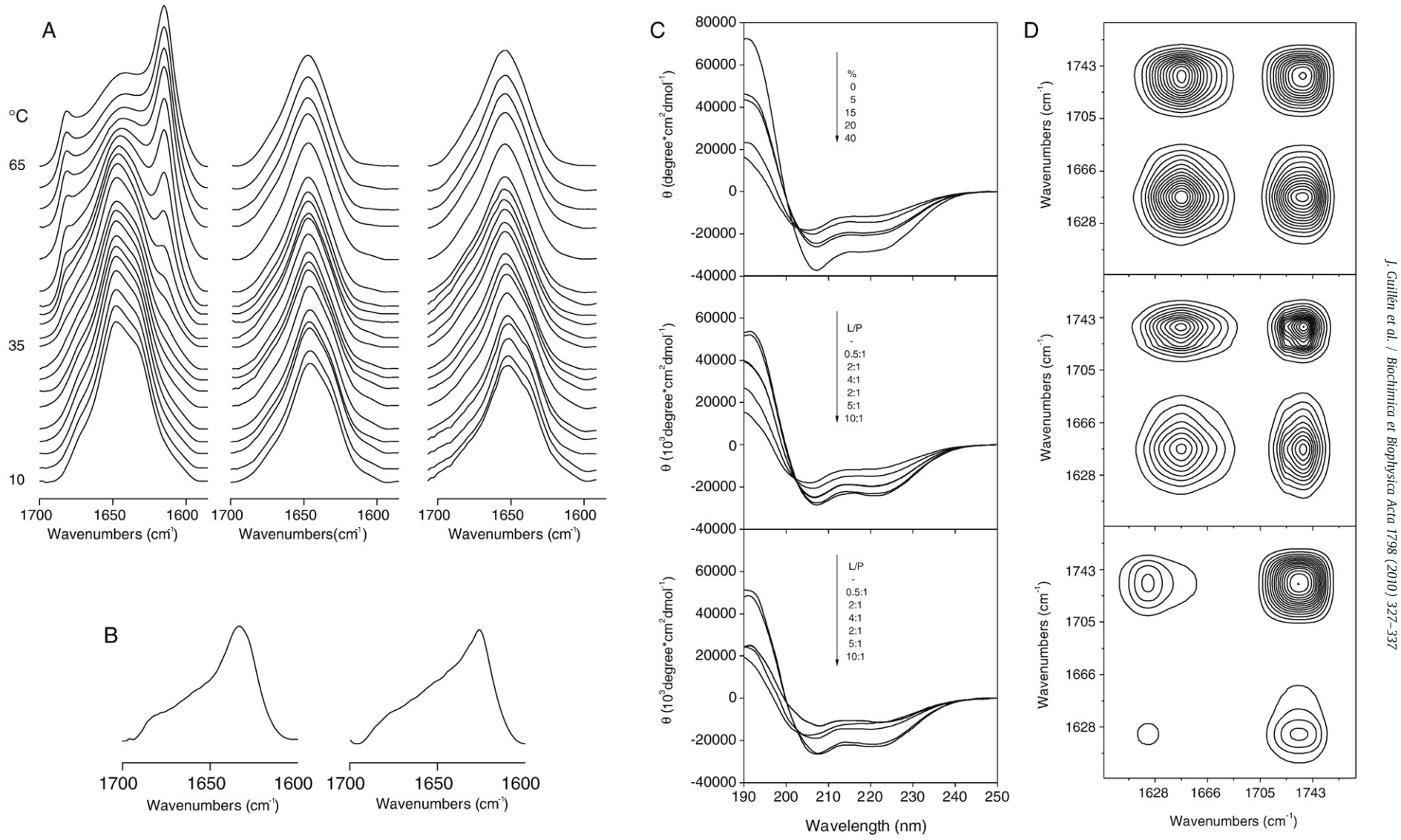

Fig. 7. (A) Stacked infrared spectra in the Amide I′ region of the NS4B$_{H2}$ peptide in solution (left) and in the presence of DMPC (middle) and DMPG (right) at different temperatures as indicated. (B) Infrared spectra of the scrambled peptides SC1 (left) and SC2 (right) in the presence of DMPC at 35 °C. (C) Circular dichroism spectra of the NS4B$_{H2}$ peptide in TFE (upper panel) and SUVs of DMPC and DMPG (middle and lower panels, respectively) at 25 °C. The percentages of TFE and the lipid-to-peptide ratio are indicated. (D) Synchronous 2D-infrared contour maps in the C=O and Amide I′ regions of samples containing the NS4B$_{H2}$ peptide in the presence of DMPC (upper panel) and DMPG (middle panel). The lower panel show the 2D-infrared contour map of a sample containing the SC1 peptide in the presence of DMPC. The range of temperatures used for the generation of the 2D-infrared maps were 10–65 °C. The solid and dotted lines represent positive and negative peaks, respectively. The phospholipid-to-peptide molar ratio was 15:1 in (A), (B) and (D).

(K_{SV} of 18.19 M^{-1}), assuming invariance of the Trp lifetime. In the presence of liposomes composed of EPC/Chol and EPC/BPS/Chol, the quenching of the Trp fluorescence of $NS4B_{H2}$ by acrylamide became significantly less efficient (K_{SV} values of 2.75 an 4.71 M^{-1}, respectively). However, K_{SV} values for SC1 were higher (7.53 and 9.86 M^{-1}, respectively). The SC2 peptide yielded a K_{SV} of 26.03 M^{-1} in buffer, revealing a great accessibility to the solvent. However, the extent of quenching was reduced but only in the presence of EPC/BPS/Chol liposomes (K_{SV} of 3.73 M^{-1}) and not in the presence of EPC/Chol (K_{SV} of 13.16 M^{-1}) (Table 2).

The effect of the $NS4B_{H2}$ peptide on the structural and thermotropic properties of phospholipid membranes was investigated by measuring the steady-state fluorescence anisotropy of the fluorescent probes DPH and TMA-DPH incorporated into model membranes composed of saturated synthetic phospholipids as a function of temperature (Fig. 5). For DMPC and DMPA bilayers, $NS4B_{H2}$ decreased the cooperativity of the thermal transition as well as induced an increase of the anisotropy of both DPH and TMA-DPH above the T_m of the phospholipids (Figs. 5A, B, C and D). In the case of DMPS, $NS4B_{H2}$ decreased the cooperativity of the main gel-to-liquid transition but in addition elicited a shift of about 3 °C to lower temperatures of the T_m (Figs. 5E andF). $NS4B_{H2}$, in general, was capable of decreasing the cooperativity of the transition T_m for all phospholipids, as observed by both types of probes. These results also suggest that the difference in charge between the phospholipid head-groups affects, but slightly, the peptide incorporation into the lipid bilayer, and therefore it should be located at the lipid–water interface influencing the fluidity of the phospholipids [49].

The effect of the $NS4B_{H2}$ peptide on the thermotropic phase behavior of different phospholipid multilamellar vesicles was assayed using differential scanning calorimetry (DSC) and the corresponding profiles are shown in Fig. 6. Both DMPC and DMPG MLVs which have not been extensively annealed at low temperatures display two endothermic peaks on heating, the pre-transition (12–14 °C, $L_{\beta'}$–$P_{\beta'}$) and the main transition (24 °C, $P_{\beta'}$–L_{α}). As illustrated in Fig. 6, incorporation of $NS4B_{H2}$ significantly altered the thermotropic behavior of both DMPC and DMPG, since the peptide abolished completely the pre-transition of both phospholipids. At a lipid/peptide ratio of 15:1, the main transition is apparently associated by at least two different peaks, which should be due to mixed phases. The coexistence of at least two phases would indicate that one of them would be enriched in peptide (phospholipids highly disturbed) whereas the other one would be impoverished in them (phospholipids slightly disturbed).

The existence of structural changes on the $NS4B_{H2}$ peptide induced by membrane binding was studied by analyzing the infrared Amide I′ band located between 1700 and 1600 cm^{-1} in membranes by infrared spectroscopy (Fig. 7). The Amide I′ region of the fully hydrated peptide in the buffer is shown in Fig. 7A. For the peptide in solution and at low temperatures, the Amide I′ band was asymmetric with a maximum of about 1648 cm^{-1} and two shoulders of about 1671 cm^{-1} and 1634 cm^{-1}. The band with the intensity maximum of about 1648 cm^{-1} would correspond to a mixture of unordered but also helical structures, whereas the band with the intensity maximum of about 1634 cm^{-1} would correspond to β-sheet [59,60]. At increasing temperatures, the band with a maximum of 1648 cm^{-1} decreased in intensity at the same time that two new bands at about 1682 cm^{-1} and 1616 cm^{-1} appeared (Fig. 7A). Since bands at about 1682 cm^{-1} and 1618 cm^{-1} appearing at the same time correspond to aggregated structures, these data would imply that the $NS4B_{H2}$ peptide changes from a mixture of helical, unordered and β-sheet structures at low temperatures to a mixture of mainly aggregated structures with small quantities of helical, β-sheet and unordered structures at high temperatures. This is what is already observed by band fitting of the Amide I′ envelope of $NS4B_{H2}$ peptide at two temperatures (Table 3). Furthermore, this transitional change in overall structure occurs at about 36–38 °C. In the presence of both DMPC and DMPG and at all temperatures studied (Fig. 7A), the Amide I′ envelope of the $NS4B_{H2}$ peptide was related to that found for the peptide in solution at low temperatures, suggesting a high degree of conformational stability of the peptide but only in the presence of the model membranes. The frequencies of the Amide I′ component bands for $NS4B_{H2}$ in the presence of both DMPC and DMPG were nearly identical to those found for the peptide in solution, but their intensity varied. As shown in Table 3, the peptide not only displayed high helical content but also significant unordered and β-sheet structures. These results imply that the secondary structure of the $NS4B_{H2}$ peptide is affected by its binding to the membrane. For comparison, Fig. 7B shows the Amide I′ band of peptides SC1 and SC2 in the presence of DMPC at 35 °C, where a maximum of about 1616 cm^{-1} is observed (the spectra were nearly identical both at low and high temperatures). These data demonstrates that these peptides are nearly completely aggregated in the presence of membranes, in contrast to $NS4B_{H2}$ which has a defined structure. Similarly to infrared, CD spectra show that the $NS4B_{H2}$ peptide presents a relatively high content of helical and unordered structures, but also β-sheet, in the presence of increasing amounts of either TFE, DMPC or DMPG (Fig. 7C).

We have used two-dimensional infrared spectroscopy (2D-IR) in order to get a deeper insight on the interaction between the $NS4B_{H2}$ peptide and the phospholipids in the different samples. Since, as shown above, there is one main transition at about 24 °C for both DMPC and DMPG, we have obtained 2D-infrared correlation maps at one temperature range, encompassing the gel-to-liquid crystalline phase transition of the pure phospholipids (Fig. 7D). The synchronous 2D-infrared correlation C=O and Amide I′ contour maps of $NS4B_{H2}$ in the presence of DMPC and DMPG are shown in the upper and middle panels of Fig. 7D. The most intense auto-peaks were located at 1647 and 1735 cm^{-1}, indicating that these are the frequencies at which the main changes should take place due to the interaction of the peptide with the phospholipids. The most intense cross-peak was observed at the same frequencies (1647/1735 cm^{-1}) and it was positive. These data indicate that the major secondary structure of $NS4B_{H2}$ which more significantly senses the phase transition of the phospholipids is the main secondary structure elements of the peptide, i.e., the α-helix and unordered components (band at 1647 cm^{-1}). For comparison, the synchronous 2D-infrared correlation contour map of peptide SC1 in the presence of DMPC is shown in the bottom panel of Fig. 7D. The map presents two auto-peaks, an intense one located at 1735 cm^{-1} and a less intense auto-peak at 1621 cm^{-1}, as well as a cross-peak at the same frequencies

Table 3
Secondary structure content of $NS4B_{H2}$ peptide as determined by infrared spectroscopy in solution and in the presence of phospholipids at different temperatures as indicated.

$NS4B_{H2}$ peptide		% Aggregated structures (1610–1625 cm^{-1})	% α-helix/3_{10}-helix (1650–1670 cm^{-1})	% β-sheet (1625–1639 cm^{-1})	% random (1640–1649 cm^{-1})	% β-turn (1670–1690 cm^{-1})
Buffer	15 °C	7	24	39	21	10
	50 °C	39	14	30	15	17
+ DMPC	15 °C	3	32	28	24	12
	50 °C	2	37	24	27	10
+ DMPG	15 °C	0	32	32	22	14
	50 °C	0	46	17	20	17

The values are rounded off to the nearest integer.

(1621/1735 cm^{-1}). The difference in the intensities of the auto-peaks indicates that the degree of interaction between peptide SC1 and DMPC is significantly lower than that found for peptide $NS4B_{H2}$ in the presence of the same phospholipid, confirming the data commented above.

4. Discussion

The replication and assembly of HCV has been suggested to occur in the ER or ER-derived membranes [7–9,61] where different proteins, including NS4B, play a central role in viral particle formation and budding. However, the functions of the individual proteins which participate in replication and/or assembly remain poorly understood. NS4B, a highly hydrophobic protein, has been suggested to alter ER membranes so that the HCV replication complex can be formed and therefore has a critical role in HCV formation. Since the biological roles of NS4B can be modulated by membranes, using an approach similar to that published recently [31–33], we have carried the analysis of the membrane-active regions of NS4B by observing the effect of a NS4B-derived peptide library from HCV strain 1aH77 on the integrity of different membrane model systems.

We have been capable of discerning different regions along the NS4B sequence which display distinct membranotropic properties using a peptide library derived from the NS4B protein. Although the use of peptide fragments might not fully mimic the properties of the intact protein, our results give an indication of the relative propensity of the different domains to bind, interact, and affect different model membranes. When all the membrane leakage values were taken into account, one peptide displayed significant membrane rupture activity, namely the region encompassing amino acids 1946–1964, peptide $NS4B_{H2}$ (Fig. 1B). Peptide $NS4B_{H2}$ coincides with one of the predicted amphipathic helices of the NS4B protein as stated above. The importance of this region is demonstrated by the fact that mutations in H2 abolish replication [23,29]. In this context, it is interesting to note that mutation W1963S, which lies within the H2 region, completely blocked replicon replication but did not alter the ability of NS4B to induce membrane alterations when expressed as a GFP fusion protein [29]. Consequently, we have made a comprehensive study of a peptide derived from this region, $NS4B_{H2}$, characterizing its binding and interaction with model membrane systems.

Peptide $NS4B_{H2}$ binds with high affinity to phospholipid model membranes, displaying similar binding affinities as those found for other peptides [48,49,51,62,63]. The peptide decreased the dipole potential of the membrane as well. Binding of $NS4B_{H2}$ to liposomes was further demonstrated by hydrophilic quenching probes, since $NS4B_{H2}$ was less accessible for quenching by acrylamide implying a buried location. An increase in Trp anisotropy was also observed for $NS4B_{H2}$ in the presence of phospholipid model membranes, showing a significant motional restriction. The fact that the two scrambled peptides, as shown by the fluorescence results, do not interact in the same way with the membrane supports the importance of the specificity on the primary amino acid sequence of this peptide. We have also shown that the $NS4B_{H2}$ peptide is capable of affecting the steady-state fluorescence anisotropy of fluorescent probes located into the palisade structure of the membrane, since the peptide was capable of decreasing the mobility and cooperativity of the phospholipid acyl chains when compared to the pure phospholipids. These results suggest that the difference in charge between the phospholipid head-groups affects, but slightly, the peptide incorporation into the lipid bilayer. The peptide should be located at the lipid–water interface influencing the fluidity of the phospholipids, most probably with an in-plane orientation rather than in a transmembrane position (work in progress).

The $NS4B_{H2}$ peptide was also capable of altering membrane stability causing the release of fluorescent probes, this effect being dependent on lipid composition and on the lipid/peptide molar ratio. The highest CF release was observed for liposomes containing zwitterionic phospholipids, although significant leakage values were also observed for liposomes composed of negatively charged phospholipids. The specific disrupting effect should be due primarily to hydrophobic interactions within the bilayer, although the specific charge of the phospholipid head-groups affects, although slightly, the extent of membrane leakage. $NS4B_{H2}$ was also capable of releasing bigger size molecules, although at smaller rates, implying that pores might be formed in the membrane but leading to the complete disruption of the membrane. Scrambled peptides induced membrane leakage but to a lesser extent. All these data demonstrate that peptide $NS4B_{H2}$ interacts more significantly with liposomes than the scrambled peptides ones, implying a specific effect of the $NS4B_{H2}$ sequence. Supposing that the solution structure is mainly an α-helix, the charged residues are located in one spot of the helix, whereas the non-polar ones are distributed uniformly along it (Fig. 1C).

The infrared spectra of the Amide I′ region of the fully hydrated peptide in buffer changed significantly with temperature. However, in the presence of membranes, it did not change, demonstrating a high stability of its conformation, where a mixture of α-helix, β-sheet and random structures coexisted. These results imply that the secondary structure of the $NS4B_{H2}$ peptide is affected by its binding to the membrane, so that membrane binding modulates the secondary structure of the peptide as it has been suggested for other peptides [48,49,51]. It should be recalled that aggregated structures were only observed for the scrambled peptides in the presence of membranes. This can be due to the change of the disposition of the charged amino acids to locations where they disrupt the hydrophobic surface of the peptide (see Fig. 1C). Interestingly, a specific interaction between $NS4B_{H2}$ and the phospholipid molecules was observed by 2D-IR.

Identifying regions within viral proteins is critical to understand and characterize the infection process. The binding to the surface and the modulation of the phospholipid biophysical properties which take place when $NS4B_{H2}$ is bound to the membrane, i.e., partitioning into the membrane surface and perturbation of the bilayer architecture, could be related to the conformational changes which might occur during the biological activity of the NS4B protein. The conservation of its structure as well as its physical and chemical properties should be essential in its function, since changes in the primary sequence cause the disruption of the hydrophobicity along the structure and prevent the resulting peptide from interacting with the membrane. Therefore, the NS4B region where the $NS4B_{H2}$ peptide resides might have an essential role in the membrane replication and/or assembly of the viral particle through the modulation of the replication complex. Consequently, our findings identify an important region in the HCV NS4B protein which might be directly implicated in the HCV life cycle.

Acknowledgements

This work was supported by grants BFU2005-00186-BMC and BFU2008-02617-BMC (Ministerio de Ciencia y Tecnología, Spain) to J.V. A.G.A was a recipient of a fellowship from the Autonomous Government of the Comunidad Valenciana, Spain. We thank Drs. Morita and Ozaki for making available the 2D-Shige program for 2D-IR. We are especially grateful to the National Institutes of Health AIDS Research and Reference Reagent Program, Division of AIDS, NIAID, NIH, for the peptides used in this work.

References

[1] M.J. Alter, Epidemiology of hepatitis C, Hepatology 26 (1997) 62S–65S.
[2] Hepatitis C—global prevalence (update), Wkly. Epidemiol. Rec. 75 (2000) 18–19.
[3] S.A. Sarbah, Z.M. Younossi, Hepatitis C: an update on the silent epidemic, J. Clin. Gastroenterol. 30 (2000) 125–143.
[4] Global surveillance and control of hepatitis C. Report of a WHO Consultation organized in collaboration with the Viral Hepatitis Prevention Board, Antwerp, Belgium, J. Viral Hepat. 6 (1999) 35–47.

[5] C. Vauloup-Fellous, V. Pene, J. Garaud-Aunis, F. Harper, S. Bardin, Y. Suire, E. Pichard, A. Schmitt, P. Sogni, G. Pierron, P. Briand, A.R. Rosenberg, Signal peptide peptidase-catalyzed cleavage of hepatitis C virus core protein is dispensable for virus budding but destabilizes the viral capsid, J. Biol. Chem. 281 (2006) 27679–27692.
[6] M.E. Major, B. Rehermann, S.M. Feinstone, Hepatitis C viruses, in: D.M. Knipe, P.M. Howley (Eds.), Fields Virology, Lippincott Williams and Wilkins, Philadelphia, PA, 2001, pp. 1127–1161.
[7] N. El-Hage, G. Luo, Replication of hepatitis C virus RNA occurs in a membrane-bound replication complex containing nonstructural viral proteins and RNA, J. Gen. Virol. 84 (2003) 2761–2769.
[8] R. Gosert, D. Egger, V. Lohmann, R. Bartenschlager, H.E. Blum, K. Bienz, D. Moradpour, Identification of the hepatitis C virus RNA replication complex in Huh-7 cells harboring subgenomic replicons, J. Virol. 77 (2003) 5487–5492.
[9] G. Mottola, G. Cardinali, A. Ceccacci, C. Trozzi, L. Bartholomew, M.R. Torrisi, E. Pedrazzini, S. Bonatti, G. Migliaccio, Hepatitis C virus nonstructural proteins are localized in a modified endoplasmic reticulum of cells expressing viral subgenomic replicons, Virology 293 (2002) 31–43.
[10] M. Dimitrova, I. Imbert, M.P. Kieny, C. Schuster, Protein–protein interactions between hepatitis C virus nonstructural proteins, J. Virol. 77 (2003) 5401–5414.
[11] M. Hijikata, Y.K. Shimizu, H. Kato, A. Iwamoto, J.W. Shih, H.J. Alter, R.H. Purcell, H. Yoshikura, Equilibrium centrifugation studies of hepatitis C virus: evidence for circulating immune complexes, J. Virol. 67 (1993) 1953–1958.
[12] P. Gallinari, D. Brennan, C. Nardi, M. Brunetti, L. Tomei, C. Steinkuhler, R. De Francesco, Multiple enzymatic activities associated with recombinant NS3 protein of hepatitis C virus, J. Virol. 72 (1998) 6758–6769.
[13] A. Grakoui, D.W. McCourt, C. Wychowski, S.M. Feinstone, C.M. Rice, Characterization of the hepatitis C virus-encoded serine proteinase: determination of proteinase-dependent polyprotein cleavage sites, J. Virol. 67 (1993) 2832–2843.
[14] D.W. Kim, Y. Gwack, J.H. Han, J. Choe, C-terminal domain of the hepatitis C virus NS3 protein contains an RNA helicase activity, Biochem. Biophys. Res. Commun. 215 (1995) 160–166.
[15] S.L. Tan, M.G. Katze, How hepatitis C virus counteracts the interferon response: the jury is still out on NS5A, Virology 284 (2001) 1–12.
[16] M.J. Gale Jr., M.J. Korth, N.M. Tang, S.L. Tan, D.A. Hopkins, T.E. Dever, S.J. Polyak, D.R. Gretch, M.G. Katze, Evidence that hepatitis C virus resistance to interferon is mediated through repression of the PKR protein kinase by the nonstructural 5A protein, Virology 230 (1997) 217–227.
[17] N. Enomoto, I. Sakuma, Y. Asahina, M. Kurosaki, T. Murakami, C. Yamamoto, Y. Ogura, N. Izumi, F. Marumo, C. Sato, Mutations in the nonstructural protein 5A gene and response to interferon in patients with chronic hepatitis C virus 1b infection, N. Engl. J. Med. 334 (1996) 77–81.
[18] S.E. Behrens, L. Tomei, R. De Francesco, Identification and properties of the RNA-dependent RNA polymerase of hepatitis C virus, EMBO J. 15 (1996) 12–22.
[19] V. Lohmann, F. Korner, U. Herian, R. Bartenschlager, Biochemical properties of hepatitis C virus NS5B RNA-dependent RNA polymerase and identification of amino acid sequence motifs essential for enzymatic activity, J. Virol. 71 (1997) 8416–8428.
[20] T. Yamashita, S. Kaneko, Y. Shirota, W. Qin, T. Nomura, K. Kobayashi, S. Murakami, RNA-dependent RNA polymerase activity of the soluble recombinant hepatitis C virus NS5B protein truncated at the C-terminal region, J. Biol. Chem. 273 (1998) 15479–15486.
[21] T. Hugle, F. Fehrmann, E. Bieck, M. Kohara, H.G. Krausslich, C.M. Rice, H.E. Blum, D. Moradpour, The hepatitis C virus nonstructural protein 4B is an integral endoplasmic reticulum membrane protein, Virology 284 (2001) 70–81.
[22] G.Y. Yu, K.J. Lee, L. Gao, M.M. Lai, Palmitoylation and polymerization of hepatitis C virus NS4B protein, J. Virol. 80 (2006) 6013–6023.
[23] D.M. Jones, A.H. Patel, P. Targett-Adams, J. McLauchlan, The hepatitis C virus NS4B protein can trans-complement viral RNA replication and modulates production of infectious virus, J. Virol. 83 (2009) 2163–2177.
[24] D. Egger, B. Wolk, R. Gosert, L. Bianchi, H.E. Blum, D. Moradpour, K. Bienz, Expression of hepatitis C virus proteins induces distinct membrane alterations including a candidate viral replication complex, J. Virol. 76 (2002) 5974–5984.
[25] M. Lundin, M. Monne, A. Widell, G. Von Heijne, M.A. Persson, Topology of the membrane-associated hepatitis C virus protein NS4B, J. Virol. 77 (2003) 5428–5438.
[26] M. Elazar, P. Liu, C.M. Rice, J.S. Glenn, An N-terminal amphipathic helix in hepatitis C virus (HCV) NS4B mediates membrane association, correct localization of replication complex proteins, and HCV RNA replication, J. Virol. 78 (2004) 11393–11400.
[27] M. Lundin, H. Lindstrom, C. Gronwall, M.A. Persson, Dual topology of the processed hepatitis C virus protein NS4B is influenced by the NS5A protein, J. Gen. Virol. 87 (2006) 3263–3272.
[28] C. Welsch, M. Albrecht, J. Maydt, E. Herrmann, M.W. Welker, C. Sarrazin, A. Scheidig, T. Lengauer, S. Zeuzem, Structural and functional comparison of the non-structural protein 4B in *Flaviviridae*, J. Mol. Graph. Model. 26 (2007) 546–557.
[29] H. Lindstrom, M. Lundin, S. Haggstrom, M.A. Persson, Mutations of the Hepatitis C virus protein NS4B on either side of the ER membrane affect the efficiency of subgenomic replicons, Virus Res. 121 (2006) 169–178.
[30] A.J. Perez-Berna, A.S. Veiga, M.A. Castanho, J. Villalain, Hepatitis C virus core protein binding to lipid membranes: the role of domains 1 and 2, J. Viral. Hepat. 15 (2008) 346–356.
[31] J. Guillen, A.J. Perez-Berna, M.R. Moreno, J. Villalain, Identification of the membrane-active regions of the severe acute respiratory syndrome coronavirus spike membrane glycoprotein using a 16/18-mer peptide scan: implications for the viral fusion mechanism, J. Virol. 79 (2005) 1743–1752.
[32] A.J. Perez-Berna, M.R. Moreno, J. Guillen, A. Bernabeu, J. Villalain, The membrane-active regions of the hepatitis C virus E1 and E2 envelope glycoproteins, Biochemistry 45 (2006) 3755–3768.
[33] M.R. Moreno, M. Giudici, J. Villalain, The membranotropic regions of the endo and ecto domains of HIV gp41 envelope glycoprotein, Biochim. Biophys. Acta 1758 (2006) 111–123.
[34] A.J. Perez-Berna, J. Guillen, M.R. Moreno, A. Bernabeu, G. Pabst, P. Laggner, J. Villalain, Identification of the membrane-active regions of hepatitis C virus p7 protein: biophysical characterization of the loop region, J. Biol. Chem. 283 (2008) 8089–8101.
[35] W.K. Surewicz, H.H. Mantsch, D. Chapman, Determination of protein secondary structure by Fourier transform infrared spectroscopy: a critical assessment, Biochemistry 32 (1993) 389–394.
[36] Y.P. Zhang, R.N. Lewis, R.S. Hodges, R.N. McElhaney, FTIR spectroscopic studies of the conformation and amide hydrogen exchange of a peptide model of the hydrophobic transmembrane alpha-helices of membrane proteins, Biochemistry 31 (1992) 11572–11578.
[37] A.G. Krainev, D.A. Ferrington, T.D. Williams, T.C. Squier, D.J. Bigelow, Adaptive changes in lipid composition of skeletal sarcoplasmic reticulum membranes associated with aging, Biochim. Biophys. Acta 1235 (1995) 406–418.
[38] T.W. Keenan, D.J. Morre, Phospholipid class and fatty acid composition of Golgi apparatus isolated from rat liver and comparison with other cell fractions, Biochemistry 9 (1970) 19–25.
[39] L.D. Mayer, M.J. Hope, P.R. Cullis, Vesicles of variable sizes produced by a rapid extrusion procedure, Biochim. Biophys. Acta 858 (1986) 161–168.
[40] C.S.F. Böttcher, C.M. Van Gent, C. Fries, A rapid and sensitive sub-micro phosphorus determination. Anal. Chim. Acta 1061 (1961) 203–204.
[41] H. Edelhoch, Spectroscopic determination of tryptophan and tyrosine in proteins, Biochemistry 6 (1967) 1948–1954.
[42] A. Bernabeu, J. Guillen, A.J. Perez-Berna, M.R. Moreno, J. Villalain, Structure of the C-terminal domain of the pro-apoptotic protein Hrk and its interaction with model membranes, Biochim. Biophys. Acta 1768 (2007) 1659–1670.
[43] M.R. Moreno, J. Guillen, A.J. Perez-Berna, D. Amoros, A.I. Gomez, A. Bernabeu, J. Villalain, Characterization of the Interaction of Two Peptides from the N Terminus of the NHR Domain of HIV-1 gp41 with Phospholipid Membranes, Biochemistry 46 (2007) 10572–10584.
[44] M.R. Eftink, C.A. Ghiron, Exposure of tryptophanyl residues and protein dynamics, Biochemistry 16 (1977) 5546–5551.
[45] T. Lefevre, K. Arseneault, M. Pezolet, Study of protein aggregation using two-dimensional correlation infrared spectroscopy and spectral simulations, Biopolymers 73 (2004) 705–715.
[46] W.C. Wimley, S.H. White, Experimentally determined hydrophobicity scale for proteins at membrane interfaces, Nat. Struct. Biol. 3 (1996) 842–848.
[47] S.H. White, W.C. Wimley, Membrane protein folding and stability: physical principles, Annu. Rev. Biophys. Biomol. Struct. 28 (1999) 319–365.
[48] R. Pascual, M. Contreras, A. Fedorov, M. Prieto, J. Villalain, Interaction of a peptide derived from the N-heptad repeat region of gp41 Env ectodomain with model membranes. Modulation of phospholipid phase behavior, Biochemistry 44 (2005) 14275–14288.
[49] L.M. Contreras, F.J. Aranda, F. Gavilanes, J.M. Gonzalez-Ros, J. Villalain, Structure and interaction with membrane model systems of a peptide derived from the major epitope region of HIV protein gp41: implications on viral fusion mechanism, Biochemistry 40 (2001) 3196–3207.
[50] N.C. Santos, M. Prieto, M.A. Castanho, Interaction of the major epitope region of HIV protein gp41 with membrane model systems. A fluorescence spectroscopy study, Biochemistry 37 (1998) 8674–8682.
[51] R. Pascual, M.R. Moreno, J. Villalain, A peptide pertaining to the loop segment of human immunodeficiency virus gp41 binds and interacts with model biomembranes: implications for the fusion mechanism, J. Virol. 79 (2005) 5142–5152.
[52] J. Cladera, I. Martin, P. O'Shea, The fusion domain of HIV gp41 interacts specifically with heparan sulfate on the T-lymphocyte cell surface, EMBO J. 20 (2001) 19–26.
[53] P. O'Shea, Intermolecular interactions with/within cell membranes and the trinity of membrane potentials: kinetics and imaging, Biochem. Soc. Trans. 31 (2003) 990–996.
[54] J. Cladera, P. O'Shea, Intramembrane molecular dipoles affect the membrane insertion and folding of a model amphiphilic peptide, Biophys. J. 74 (1998) 2434–2442.
[55] T.C. Laurent, K.A. Granath, Fractionation of dextran and Ficoll by chromatography on Sephadex G-200, Biochim. Biophys. Acta 136 (1967) 191–198.
[56] D.B. Fisher, C.E. Cash-Clark, Sieve tube unloading and post-phloem transport of fluorescent tracers and proteins injected into sieve tubes via severed aphid stylets, Plant. Physiol. 123 (2000) 125–138.
[57] L. Yang, T.A. Harroun, T.M. Weiss, L. Ding, H.W. Huang, Barrel-stave model or toroidal model? A case study on melittin pores, Biophys. J. 81 (2001) 1475–1485.
[58] D. Allende, S.A. Simon, T.J. McIntosh, Melittin-induced bilayer leakage depends on lipid material properties: evidence for toroidal pores, Biophys. J. 88 (2005) 1828–1837.
[59] J.L. Arrondo, F.M. Goni, Structure and dynamics of membrane proteins as studied by infrared spectroscopy, Prog. Biophys. Mol. Biol. 72 (1999) 367–405.
[60] D.M. Byler, H. Susi, Examination of the secondary structure of proteins by deconvolved FTIR spectra, Biopolymers 25 (1986) 469–487.
[61] M. Ait-Goughoulte, C. Hourioux, R. Patient, S. Trassard, D. Brand, P. Roingeard, Core protein cleavage by signal peptide peptidase is required for hepatitis C virus-like particle assembly, J. Gen. Virol. 87 (2006) 855–860.
[62] O. Korazim, K. Sackett, Y. Shai, Functional and structural characterization of HIV-1 gp41 ectodomain regions in phospholipid membranes suggests that the fusion-active conformation is extended, J. Mol. Biol. 364 (2006) 1103–1117.
[63] M. Rabenstein, Y.K. Shin, A peptide from the heptad repeat of human immunodeficiency virus gp41 shows both membrane binding and coiled-coil formation, Biochemistry 34 (1995) 13390–13397.